

Article (refereed) - postprint

Comyn-Platt, Edward; Hayman, Garry; Huntingford, Chris; Chadburn, Sarah E.; Burke, Eleanor J.; Harper, Anna B.; Collins, William J.; Webber, Christopher P.; Powell, Tom; Cox, Peter M.; Gedney, Nicola; Sitch, Stephen. 2018. **Carbon budgets for 1.5 and 2°C targets lowered by natural wetland and permafrost feedbacks.** *Nature Geoscience*, 11 (8). 568-573.

<https://doi.org/10.1038/s41561-018-0174-9>

© 2018 Springer Nature Limited

This version available <http://nora.nerc.ac.uk/id/eprint/520608/>

NERC has developed NORA to enable users to access research outputs wholly or partially funded by NERC. Copyright and other rights for material on this site are retained by the rights owners. Users should read the terms and conditions of use of this material at

<http://nora.nerc.ac.uk/policies.html#access>

This document is the author's final manuscript version of the journal article, incorporating any revisions agreed during the peer review process. There may be differences between this and the publisher's version. You are advised to consult the publisher's version if you wish to cite from this article.

www.nature.com/

Contact CEH NORA team at
noraceh@ceh.ac.uk

1 **Carbon budgets for 1.5 and 2°C targets lowered by natural wetland** 2 **and permafrost feedbacks**

3 Edward Comyn-Platt^{*}, Garry Hayman¹, Chris Huntingford¹, Sarah Chadburn^{2,3}, Eleanor
4 Burke⁴, Anna B. Harper³, William Collins⁵, Christopher Webber⁵, Tom Powell³, Peter M.
5 Cox³, Nicola Gedney⁶, Stephen Sitch³

6 1: Centre for Ecology and Hydrology, Wallingford, OX10 8BB, U.K.

7 2: University of Leeds, Leeds, LS2 9JT, U.K.

8 3: University of Exeter, Exeter, EX4 4QF, U.K.

9 4: Met Office Hadley Centre, FitzRoy Road, Exeter, EX1 3PB, U.K.

10 5: University of Reading, Reading, RG6 6BB, U.K.

11 6: Met Office Hadley Centre, Joint Centre for Hydrometeorological Research, Wallingford,
12 OX10 8BB, U.K.

13 * Corresponding Author

14 **Keywords: Climate stabilisation, global warming, temperature thresholds, carbon cycle,**
15 **methane cycle, permafrost thaw**

16 **Global methane emissions from natural wetlands and carbon release from permafrost**
17 **thaw have a positive feedback on climate, yet are not represented in most state-of-the-art**
18 **climate models. Furthermore, a fraction of the thawed permafrost carbon is released as**
19 **methane, enhancing the combined feedback strength. We present simulations with an**
20 **inverted intermediate complexity climate model which follow prescribed global warming**
21 **pathways to stabilisation at 1.5°C or 2.0°C above pre-industrial levels by the year 2100,**
22 **and that incorporates a state-of-the-art global land surface model with updated**
23 **descriptions of wetland and permafrost carbon release. We demonstrate that the climate**
24 **feedbacks from those two processes are substantial. Specifically, permissible**
25 **anthropogenic fossil fuel CO₂ emission budgets are reduced by 17-23% (47-56 GtC) for**
26 **stabilisation at 1.5°C, and 9-13% (52-57 GtC) for 2.0°C stabilisation. In our simulations**
27 **these feedback processes respond faster at temperatures below 1.5°C, and the differences**
28 **between the 1.5°C and 2°C targets are disproportionately small. This key finding is due**

29 **to our interest in transient emission pathways to the year 2100 and does not consider the**
30 **longer term implications of these feedback processes. We conclude that natural feedback**
31 **processes from wetlands and permafrost must be considered in assessments of transient**
32 **emission pathways to limit global warming.**

33 **Background**

34 The 2009 meeting of the United Nations' Framework Convention on Climate Change
35 (UNFCCC) in Copenhagen formalised the aspiration to stabilise global warming at no more
36 than 2°C above pre-industrial levels¹. The subsequent UNFCCC Paris Agreement in 2015
37 raised the additional possibility of aiming for an even lower upper warming threshold of 1.5°C².
38 These targets will require large reductions in anthropogenic greenhouse gas (GHG) emissions,
39 with sustained decreases of ~3% per annum^{3,4} and development of technologies to remove
40 carbon dioxide (CO₂) from the atmosphere. This is because the equilibrium global warming for
41 current GHG concentrations may already be near 1.5°C⁵. Given the anticipated difficulty in
42 keeping below the 1.5°C threshold, two key questions are being asked. First, what are the
43 implications in terms of allowable anthropogenic emissions to keep warming below 1.5°C
44 rather than 2.0°C? Second, what is gained climatically or environmentally by keeping below
45 1.5°C, i.e. are unwelcome climate impacts potentially avoided?

46 The climate change observed during recent decades has been strongly linked to human
47 influences on atmospheric GHG composition, leading the 5th IPCC assessment to state: “it is
48 extremely likely that human influence has been the dominant cause of the observed warming
49 since the mid-20th century”⁶. However atmospheric GHG levels are affected both directly (via
50 anthropogenic GHG emissions) and indirectly by human activity. Indirect effects include
51 climate change-induced adjustments to land-atmosphere and/or ocean-atmosphere GHG
52 exchange fluxes. This was first modelled for the global carbon cycle by [7] who predicted a

53 significant flux of carbon to the atmosphere via increased ecosystem respiration under warming
54 for a business-as-usual scenario. Similar analyses have been undertaken separately for
55 additional methane (CH₄) release from wetlands^{8,9} and additional carbon released from the
56 long-term permafrost store¹⁰⁻¹². The increase in global warming may be under-estimated for a
57 prescribed anthropogenic emissions trajectory if these processes are not considered. In
58 reference to policy questions, the anthropogenic fossil fuel emission budgets (AFFEBs) to limit
59 global warming to 1.5°C or 2.0°C may be significantly reduced from current assessments^{6,13,14}.

60 This research focusses on two feedback processes which were not included in most models in
61 the fifth phase of the Coupled Model Intercomparison Project (CMIP5)¹⁵ and will only be
62 included in a small fraction of models participating the sixth phase (CMIP6). These are the
63 effects of carbon release from the permafrost store as CO₂ and the increased CH₄ emissions
64 from natural wetlands, and the coupling between the two effects where carbon from thawed
65 permafrost is also released as CH₄^{16,17}. These are particularly pertinent issues given that CH₄
66 has a larger Global Warming Potential (GWP) by equivalent weight than CO₂, and the recent
67 resurgent growth in atmospheric CH₄¹⁸.

68 In contrast to the CMIP5 simulations, which modelled climatic and environmental responses
69 to prescribed atmospheric concentration pathways, the objective here is to quantify the
70 anthropogenic response required to meet a specified global warming target. We develop an
71 inverted form of climate model that follows prescribed temperature trajectories¹⁹ and calculate
72 corresponding AFFEBs¹³, including the two aforementioned feedback effects. The modelling
73 framework is based on the coupled Joint UK Land Environment Simulator (JULES^{20,21}) and
74 Integrated Model Of Global Effects of climatic aNomalies (IMOGEN^{22,23}) system (Methods).
75 The approach taken is generic and may be employed in further research to answer a number of
76 environmental policy related questions in terms of meeting specified warming thresholds.

77 **Model Setup**

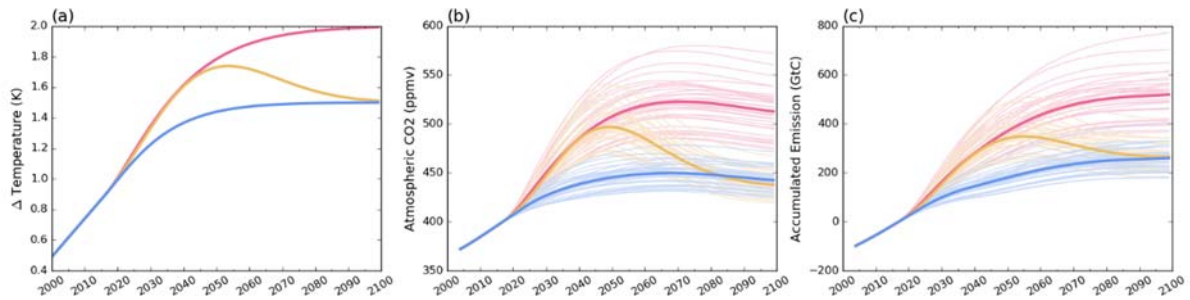
78 We use JULES version-4.8 release, with the addition of a 14 layered soil column for both
79 hydro-thermal²⁴ and carbon²⁵ dynamics. The JULES configuration includes representations of
80 land-use and land-use change (LULUC) and ozone damage on plant stomata to address policy-
81 relevant warming scenarios outside the scope of this paper. (Methods)

82 The major advancement in the IMOGEN configuration used for this study is the prescription
83 of evolving global temperature trajectories. Following this inverted form (Figure SI.1b),
84 changes in radiative forcing, ΔQ , are calculated as a function of the time-history of global
85 warming which are then ascribed to compatible atmospheric compositions of GHGs. The
86 anthropogenic contribution to atmospheric CO₂ is calculated whilst taking in to account
87 changes to the land and ocean carbon stores, together with prescription or calculation of non-
88 CO₂ greenhouse gases. Additional IMOGEN enhancements for this analysis include the
89 calculation of atmospheric CH₄ concentration and effective radiative forcing, capturing the
90 climate impacts on CH₄ release from natural wetlands. (Methods)

91 Critical to our analysis is understanding emission pathways available to stabilise at either 1.5°C
92 or 2.0°C of warming since pre-industrial times. As this will be strongly influenced by
93 anthropogenic perturbation of the climate system to present day, we constrain the historical
94 global temperature (ΔT_G) to the HadCRUT4 observational record²⁶ and atmospheric
95 composition to the Representative-Concentration-Pathway (RCP) record²⁷ for the period 1850-
96 2015. Future projections of the non-CO₂ atmospheric composition is taken from the IMAGE-
97 3.0 implementation of Shared-Socioeconomic-Pathway (SSP) version-2 under RCP2.6
98 (SSP2_RCP-2.6_IMAGE)²⁸. (Methods)

99 We select three global warming pathways to stabilisation at the 1.5°C or 2.0°C targets by 2100

100 (

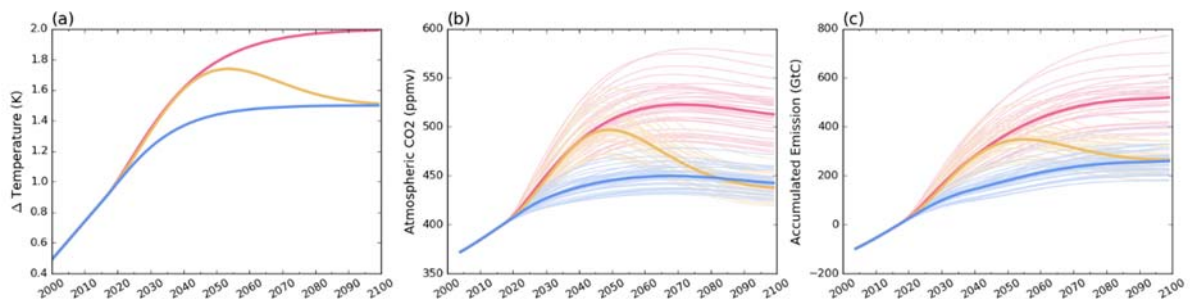


101

102 Figure 1a and SI.2), which are described using the formulation in [19] (Methods). Two of the
103 considered trajectories reach asymptotes at 1.5°C and 2.0°C from below. The third asymptotes
104 to 1.5°C after an overshoot to 1.75°C, representing greater attempts of decarbonisation of the
105 atmosphere towards the end of the 21st century. The overshoot trajectory allows investigation
106 into hysteresis effects which may have path-dependent effects on temperature stabilisation, e.g.
107 carbon release due to permafrost thaw.

108 Discussion

109 Using our control configuration of JULES (i.e. with no natural wetland CH₄ nor permafrost
110 carbon feedbacks), we estimate the interquartile range of the AFFEBs for 2015-2100 as 464-
111 568 GtC to meet the 2°C target, and 227-283 GtC or 227-288 GtC to meet the 1.5°C target with
112 or without the overshoot, respectively (

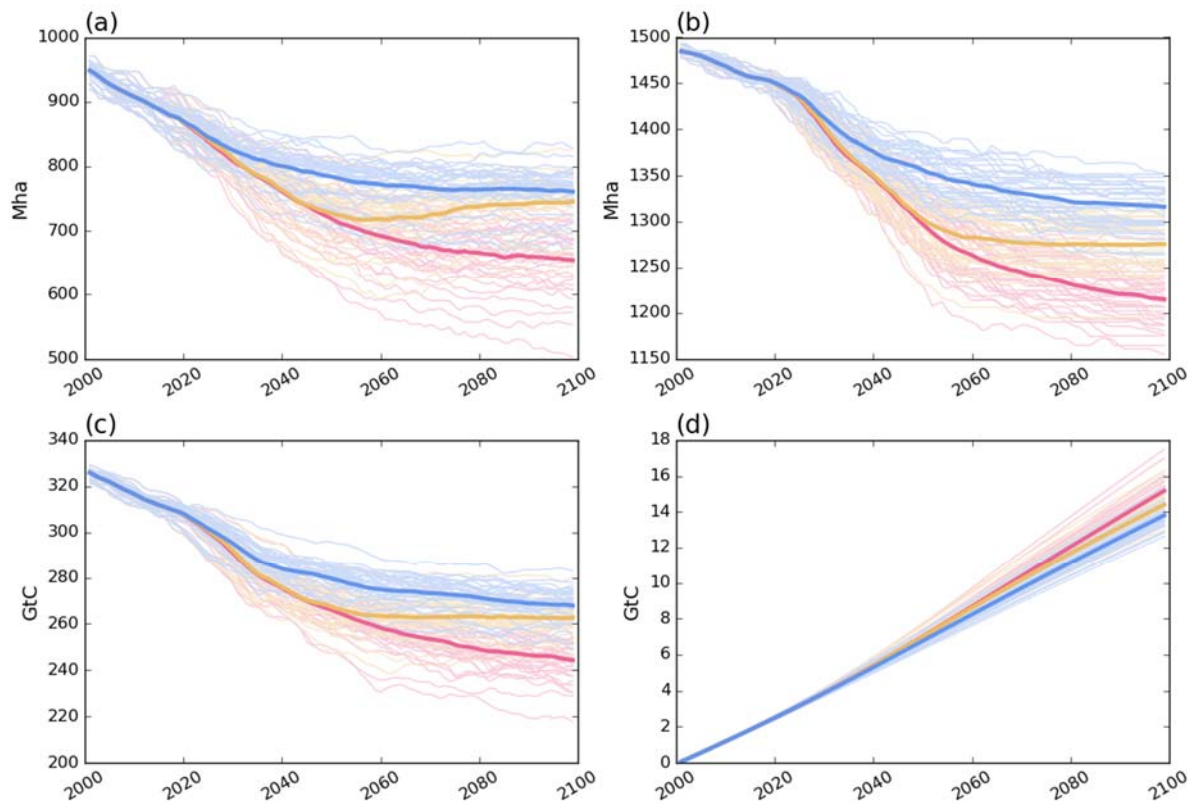


113

114 Figure 1 and Table 1). The AFFEBs are broadly linear in ΔT_G across the three scenarios, i.e.
115 378-480 GtC °C⁻¹ and 421-516 GtC °C⁻¹ for the 1.5°C and 2°C scenarios, respectively. These
116 results agree with previous estimates of AFFEBs using different methods¹³.

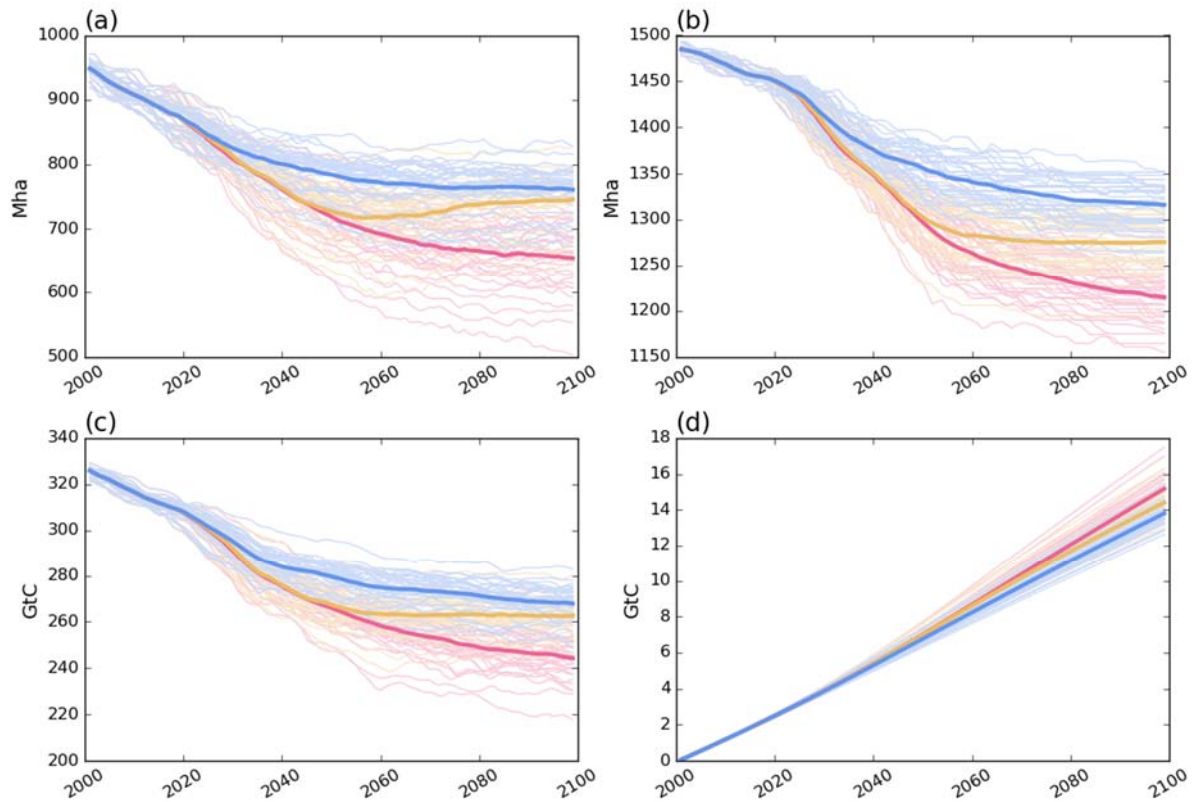
117 The 2°C scenario allows a close to “business as usual” emissions for the coming decade
118 followed by extensive emission reductions of 3.5-4.1% per year between 2030 and 2100.
119 However, if society were to act more immediately, the AFFEB could be met with year-on-year
120 reductions of 2.2-2.7% from 2020. The 1.5°C scenario with no overshoot indicates a near
121 immediate peak in annual emissions followed by 3.5-4.3% year-on-year reductions from 2020.
122 Despite the similarity of the AFFEB for the two 1.5°C scenarios, the overshoot scenario places
123 larger pressure on future generations. This pathway implies that anthropogenic activities are a
124 net 311-377 GtC source of CO₂ until the early-2050s, then must become a net sink, capturing
125 90.4-101 GtC. These estimates go further than previous attempts to quantify AFFEB^{13,14} as
126 they provide an AFFEB for each GCM, and the transient pathway, to meet the specified
127 stabilised temperature.

128 The role of permafrost thaw in modulating the AFFEB is measured as the amount of carbon
129 that was in the pre-industrial permafrost carbon store that is lost to the atmosphere. We define
130 permafrost as soil layers within grid cells which JULES simulates as perennially frozen. We
131 find our estimates of present day permafrost extent and loss rate to agree with the models
132 assessed in [11] (Figure SI.3). Furthermore, a comparison with an observation dataset²⁹
133 demonstrates that our simulations reproduce a reasonable present day spatial coverage of
134 permafrost (Figure SI.4). By 2100, the model ensemble estimates a median 138 Mha loss of
135 permafrost area at 3m depth for the 1.5°C asymptote pathway and a median 239 Mha loss for



137

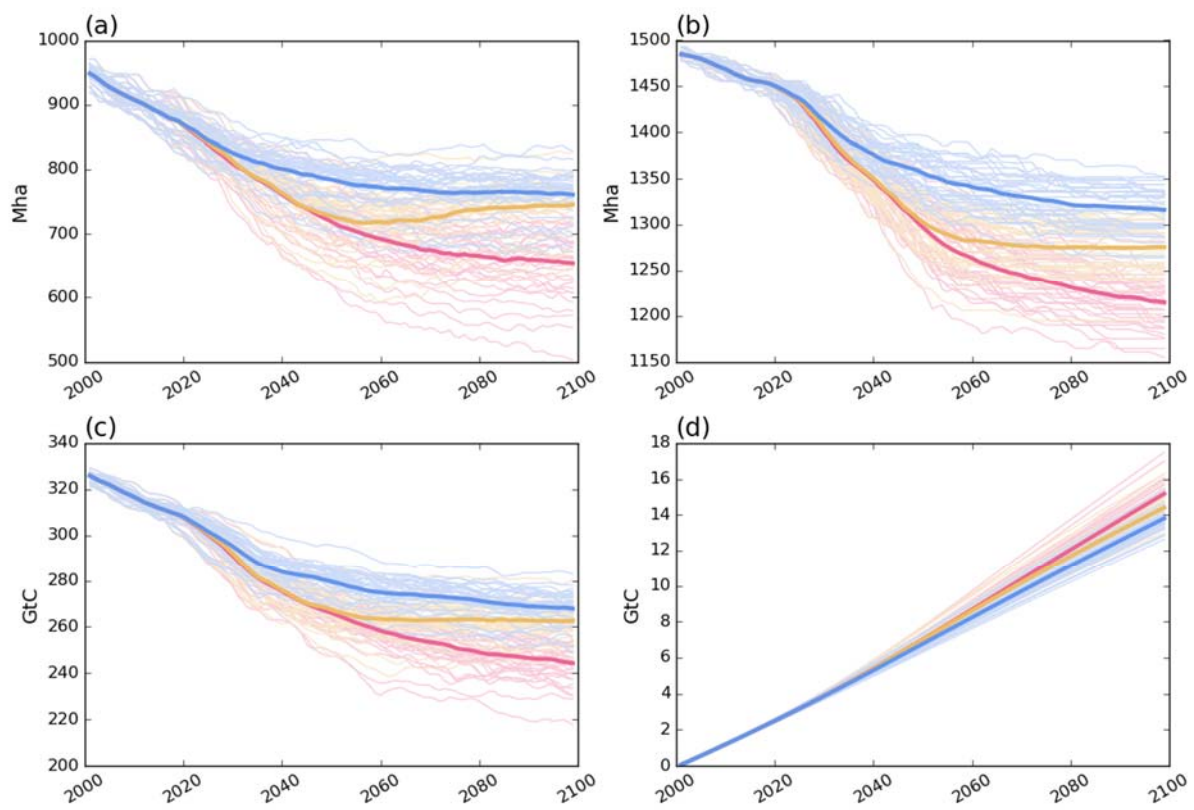
138 Figure 2a and Table SI.3). This degradation of permafrost results in an additional 40.0-46.3,
139 45.6-51.2 and 61.9-72.0 GtC of pre-industrial permafrost carbon which is no longer perennially
140 frozen, relative to 2015, for the three temperature scenarios. Between 20% and 30% of this
141 newly “thermally active” carbon has been released to the atmosphere, reducing AFFEBs by



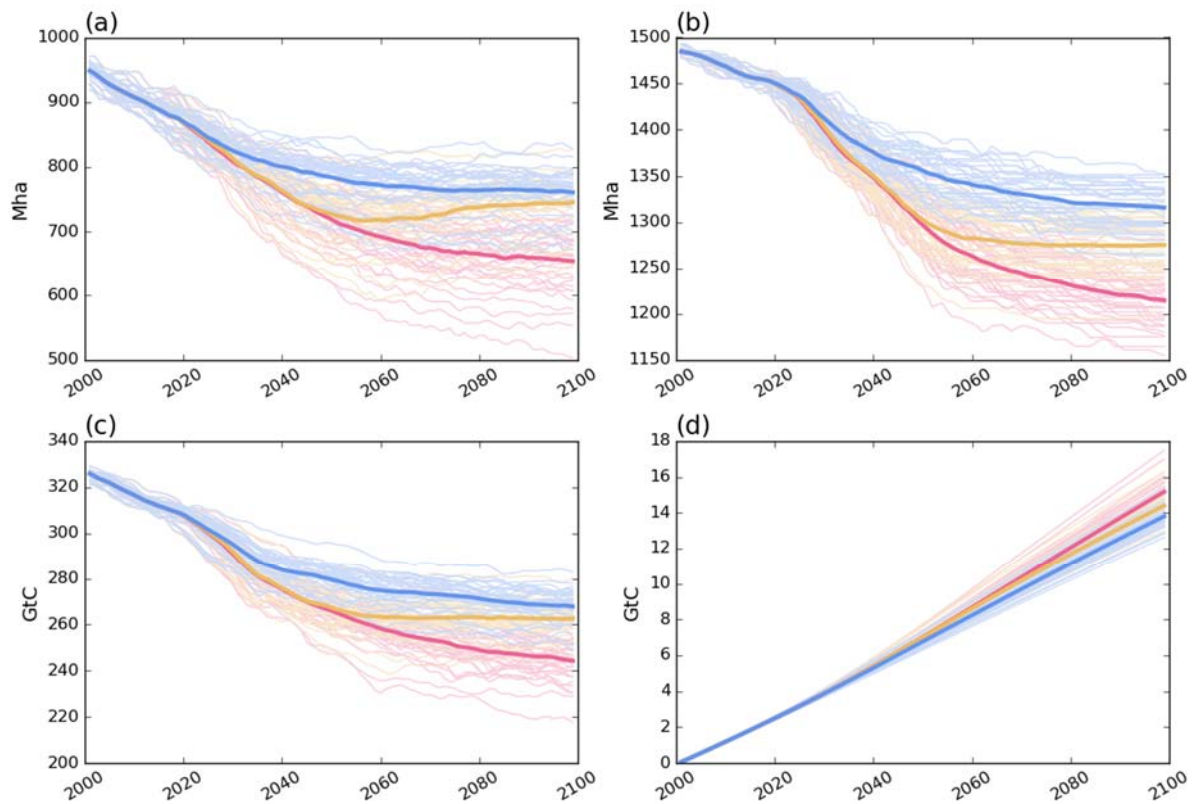
143

144 Figure 2d and Table 1– blue boxes in first column). The uncertainty range presented here is the
 145 interquartile range of the climate ensemble. We use a model configuration very close to the
 146 upper extreme of the process uncertainty presented in [10], hence our estimates represent an
 147 upper limit to the potential permafrost feedback. Applying the findings of [10] implies that a
 148 lower limit to the permafrost feedback would be roughly half of what is presented here (~5-7
 149 GtC).

150 The differences in permafrost loss between scenarios appears less than previous estimates³⁰.
 151 However, our estimates represent a transient snapshot at 2100 and not equilibrium conditions
 152 which will not be met for several centuries. The permafrost is not in equilibrium by 2100,
 153 particularly the deeper soil layers which show a lagged response to changes in the surface air



156 Figure 2a and 2b). This behaviour is similarly observed in the pre-industrial permafrost carbon
157 stocks which are still being significantly depleted by year 2100 (



158

159 Figure 2c and 2d). The loss-rate of pre-industrial permafrost carbon to the atmosphere is still
160 increasing by 2100 as the total pool of soil carbon to respire continues to grow despite the
161 stabilisation of surface air temperature. This highlights the time-scales involved in permafrost
162 processes and indicates that permafrost thaw will continue to have large implications on
163 anthropogenic emissions into the 22nd century even if temperatures have stabilised.

164 The response of the AFFEB to permafrost thaw is non-linear with respect to ΔT_G , i.e. 19.3-21.7
165 GtC °C⁻¹ for the 1.5°C scenarios and 11.6-12.5 GtC °C⁻¹ for the 2°C scenario. This implies that
166 the permafrost feedback is faster at lower temperature changes, and keeping temperatures
167 below 1.5°C, rather than 2°C, does not make large differences to AFFEBs to 2100. However,
168 this behaviour is primarily a feature of our interest in the AFFEB to 2100 and the additional
169 carbon released in the 2°C scenario will continue to have implications into the 22nd century.

170 The impact of the natural wetland CH₄ feedback on the AFFEBs is the sum of reduced carbon
171 uptake of the atmosphere, ocean and land due to a higher atmospheric CH₄ concentration. The
172 magnitude and distribution of the JULES natural wetland CH₄ emissions are driven primarily
173 by wetland area and the soil temperature and carbon content (Methods). Our estimates of
174 wetland extent and zonal distribution for the present day are within the range of state-of-the-
175 art observation datasets^{31,32} (Figure SI.4). To encapsulate a range of methanogenesis process
176 uncertainty we include a temperature sensitivity ensemble by varying Q₁₀ in Equation 1
177 (Methods). We use Q₁₀ values calibrated to represent two wetland types identified in [33]
178 (“poor-fen” and “rich-fen”) and a third “low-Q₁₀” which gave increased importance to high
179 latitude emissions (Methods). Our ensemble spread sufficiently describes the magnitude and
180 distribution of present day CH₄ emissions from natural wetlands according to the models
181 assessed in a recent intercomparison study³⁴ (Figure SI.5). However, there is still much
182 uncertainty in natural wetland CH₄ emissions and future work will look to improve our model
183 via more rigorous comparisons with observational datasets.

184 The global mean atmospheric CH₄ concentrations are increased by 3-9% and 6-15% (w.r.t. the
185 control simulation) when the natural CH₄ feedback is included for the 1.5°C and 2°C target,
186 respectively (Figure 3a for the “poor-fen” parameterisation and supplementary Figure SI.6 for
187 the other parameterisations). The major driver of increased CH₄ emissions is increased soil
188 temperatures as changes in wetland extent and soil carbon content are not consistent globally
189 (Figure SI.7). The increased atmospheric CH₄ concentrations imply reduced atmospheric CO₂
190 concentrations to ensure that simulations follow the prescribed temperature pathway (Figure
191 3b). The reduced atmospheric CO₂ concentrations result in reduced CO₂ fertilisation of
192 vegetation and a slower oceanic drawdown of CO₂. Additionally, the increased ozone due to
193 increased CH₄ (Methods) limits productivity further still. The AFFEBs are hence lowered by

194 33-51 GtC for the full temperature sensitivity ensemble (yellow cells in Table 1 and Figure
195 3d).

196 Similar to the permafrost feedback, the natural CH₄ feedback is non-linear with respect to ΔT_G ,
197 i.e. 55-71 GtC °C⁻¹ for the 1.5°C scenario and 34-46 GtC °C⁻¹ for the 2°C scenario. The effects
198 of the natural CH₄ feedbacks are 13-21% larger for the 2°C scenario than the 1.5°C scenarios
199 despite a temperature increase that is 83% larger, from present day. Furthermore, we found that
200 this non-linear behaviour was maintained for the three temperature sensitivities considered in
201 our uncertainty analysis (Figure 3d). Therefore, in the context of the natural wetland feedback
202 strength, we conclude that constraining warming to less than 1.5°C, rather than 2°C, has a
203 disproportionately small impact on the AFFEB.

204 The natural CH₄ feedback strength is slightly reduced for the 1.5°C with overshoot in
205 comparison to the 1.5°C asymptote pathway (Figure 3a). The two scenarios have similar
206 atmospheric CH₄ concentrations by 2100 (median difference < 5ppb) hence the atmospheric
207 CO₂ sinks in year 2100 are similar. However, the overshooting pathway has higher atmospheric
208 CO₂ concentrations during the 21st Century, hence the ocean and land sinks are not reduced by
209 as much. This implies that an overshooting pathway may be more robust to the natural CH₄
210 feedback as the land and ocean sinks are more effective. Given that the magnitude of this
211 difference is small, 1-2 GtC, it is difficult to generalise this behaviour.

212 Our simulations show little interaction (where thawed permafrost is released as CH₄) between
213 the feedback processes, i.e. the difference between the sum of the AFFEB differences and
214 AFFEB difference from the simulation including both feedback processes < 2 GtC. The amount
215 of CH₄ released from the thawed permafrost carbon is 0.2-0.6 TgCH₄ per year, where the upper
216 limit corresponds to the “low-Q₁₀” parameterisation (Figure SI.8a) which gave a greater
217 emphasis to CH₄ emissions from cooler regions (methods). This is ~0.16-0.56 % of global CH₄

218 emissions in 2015, decreasing to ~0.12-0.46% in 2100 (Figure SI.8b). Similarly, the fraction
219 of permafrost carbon released as CH₄ is 0.15-0.59% (Figure SI.8c). The additional atmospheric
220 CH₄ translates to changes of global atmospheric CO₂ of the order 0.1 ppmv, which has little
221 impact on the absolute atmospheric carbon sink nor the uptake of carbon by the land and ocean.
222 Hence, in the context of our estimates of AFFEBs to meet the UNFCCC targets (200-500 GtC),
223 the interplay of these two feedback schemes is largely negligible. However, our modelling
224 framework does not account for thermokarst lakes created via ground subsidence following
225 permafrost thaw. To provide an estimate of uncertainty regarding this omission we emulate the
226 behaviour offline by linearly increasing wetland extent in permafrost regions through the 21st
227 Century, from a factor of 1 in year 2000 to a factor of 2 in year 2100 (Figure SI.10). The
228 increased CH₄ emissions reduces the AFFEB by a further 0.8-2.5 GtC. However, we see this
229 as an over-estimate as the emulation does not consider the reduced aerobic respiration due to
230 increased saturated soil which has been shown to outweigh the increased CH₄ emissions¹⁶.

231 **Conclusions**

232 The combined effect of these feedback processes has large implications on AFFEBs, 16.7-
233 23.2% (46.6-55.7 GtC) and 9.5-13% (51.4-64.6 GtC) reductions for the 1.5°C and 2°C
234 scenarios from the control runs, respectively (Table 1 – green cells). In terms of mitigation
235 pathways this corresponds to 4.6-5.4% year-on-year reductions in anthropogenic emissions
236 beginning in 2020 to meet the 1.5°C emission budget. To meet the 2°C warming target, the
237 allowable emissions would require year-on-year reductions of 3.9-4.5% beginning in 2030, or
238 2.4-3.0% starting in 2020. This represents a 1-1.5% increase in reduction rates for the 1.5°C
239 and only a 0.3-0.6% increase in reduction rates for the 2°C. The 1.5°C overshoot pathway
240 indicates that total allowable anthropogenic emissions would need to be no more than 292-351
241 GtC prior to the mid-2050s followed by a removal of 101-118 GtC.

242 We find that to fulfil a 1.5°C warming threshold with no overshoot, increased CH₄ emissions
243 from natural wetlands reduce the AFFEB between now and year 2100 by 12-17%. Carbon
244 released from the long-term permafrost store reduces the AFFEB by an additional 4.1-5.3%,
245 and the interplay between the two processes a further 0.5-1 %. This leaves AFFEBs of 175-
246 235 GtC to 2100, a total reduction of 17-23%. Allowing for an overshoot to 1.75°C, but still
247 leading ultimately to 1.5°C warming, makes little difference to the AFFEB, 172-240 GtC to
248 2100. However, such an eventuality would require significant developments of carbon capture
249 technologies in the second half of the 21st century during which the net anthropogenic
250 contribution to the carbon cycle would have to be a 101-118 GtC sink. The reduction in AFFEB
251 for stabilisation at 2.0°C is, in absolute terms, similar to the reductions required to meet the
252 1.5°C target, 51.4-64.6 GtC. However, this is a much lower fraction of the AFFEB, 9.5-13.0%.
253 Our overall findings are that the natural climate feedbacks considered here are non-linear with
254 respect to the AFFEB to meet a given temperature target by year 2100. Therefore, the role of
255 the natural CH₄ and permafrost thaw feedback processes become increasingly more important
256 when considering the lower stabilisation temperature target of 1.5°C.

257 **References**

- 258 1 UNFCCC. Copenhagen Accord FCCC/CP/2015/L.9/Rev. 1. (2009).
- 259 2 UNFCCC. Adoption of the Paris Agreement FCCC/CP/2015/L.9/Rev. 1. (2015).
- 260 3 Huntingford, C. *et al.* The link between a global 2 °C warming threshold and emissions in
261 years 2020, 2050 and beyond. *Environmental Research Letters* **7**, 014039 (2012).
- 262 4 Rogelj, J., McCollum, D. L., Reisinger, A., Meinshausen, M. & Riahi, K. Probabilistic
263 cost estimates for climate change mitigation. *Nature* **493**, 79-83 (2013).
- 264 5 Huntingford, C. & Mercado, L. M. High chance that current atmospheric greenhouse
265 concentrations commit to warmings greater than 1.5 °C over land. **6**, 30294 (2016).
- 266 6 IPCC. in *Climate Change 2013: The Physical Science Basis. Contribution of Working*
267 *Group I to the Fifth Assessment Report of the Intergovernmental Panel on Climate Change*
268 (eds T.F. Stocker *et al.*) (Cambridge University Press, 2013).
- 269 7 Cox, P. M., Betts, R. A., Jones, C. D., Spall, S. A. & Totterdell, I. J. Acceleration of global
270 warming due to carbon-cycle feedbacks in a coupled climate model. *Nature* **408**, 184-187,
271 doi:10.1038/35041539 (2000).
- 272 8 Gedney, N., Cox, P. M. & Huntingford, C. Climate feedback from wetland methane
273 emissions. *Geophysical Research Letters* **31**, doi:10.1029/2004gl020919 (2004).

- 274 9 Shindell, D. T., Walter, B. P. & Faluvegi, G. Impacts of climate change on methane
275 emissions from wetlands. *Geophysical Research Letters* **31**, L21202,
276 doi:10.1029/2004GL021009 (2004).
- 277 10 Burke, E. J. *et al.* Quantifying uncertainties of permafrost carbon–climate feedbacks.
278 *Biogeosciences* **14**, 3051 (2017).
- 279 11 McGuire, A. D. *et al.* Variability in the sensitivity among model simulations of permafrost
280 and carbon dynamics in the permafrost region between 1960 and 2009. *Global*
281 *Biogeochemical Cycles* **30**, 1015-1037, doi:10.1002/2016GB005405 (2016).
- 282 12 Burke, E. J., Chadburn, S. E., Huntingford, C. & Jones, C. D. CO₂ loss by permafrost
283 thawing implies additional emissions reductions to limit warming to 1.5 or 2 °C.
284 *Environmental Research Letters* **13**, 024024 (2018).
- 285 13 Millar, R. J. *et al.* Emission budgets and pathways consistent with limiting warming to
286 1.5°C. *Nature Geoscience*, 741-748, doi:10.1038/ngeo3031 (2017).
- 287 14 Tokarska, K. B. & Gillett, N. P. Cumulative carbon emissions budgets consistent with
288 1.5 °C global warming. *Nature Climate Change* **8**, 296-299, doi:10.1038/s41558-018-
289 0118-9 (2018).
- 290 15 Taylor, K. E., Stouffer, R. J. & Meehl, G. A. An Overview of CMIP5 and the Experiment
291 Design. *Bulletin of the American Meteorological Society* **93**, 485-498, doi:10.1175/bams-
292 d-11-00094.1 (2012).
- 293 16 Schädel, C. *et al.* Potential carbon emissions dominated by carbon dioxide from thawed
294 permafrost soils. *Nature Climate Change* **6**, 950, doi:10.1038/nclimate3054 (2016).
- 295 17 Schuur, E. A. G. *et al.* Climate change and the permafrost carbon feedback. *Nature* **520**,
296 171-179, doi:10.1038/nature14338 (2015).
- 297 18 Crill, P. M. & Thornton, B. F. Whither methane in the IPCC process? *Nature Climate*
298 *Change* **7**, 678, doi:10.1038/nclimate3403 (2017).
- 299 19 Huntingford, C. *et al.* Flexible parameter-sparse global temperature time profiles that
300 stabilise at 1.5 and 2.0 °C. *Earth Syst. Dynam.* **8**, 617-626, doi:10.5194/esd-8-617-2017
301 (2017).
- 302 20 Best, M. *et al.* The Joint UK Land Environment Simulator (JULES), model description–
303 Part 1: energy and water fluxes. *Geoscientific Model Development* **4**, 677-699 (2011).
- 304 21 Clark, D. *et al.* The Joint UK Land Environment Simulator (JULES), model description–
305 Part 2: carbon fluxes and vegetation dynamics. *Geoscientific Model Development* **4**, 701-
306 722 (2011).
- 307 22 Huntingford, C. & Cox, P. M. An analogue model to derive additional climate change
308 scenarios from existing GCM simulations. *Climate Dynamics* **16**, 575-586,
309 doi:10.1007/s003820000067 (2000).
- 310 23 Huntingford, C. *et al.* IMOGEN: an intermediate complexity model to evaluate terrestrial
311 impacts of a changing climate. *Geoscientific Model Development* **3**, 679-687,
312 doi:10.5194/gmd-3-679-2010 (2010).
- 313 24 Chadburn, S. *et al.* An improved representation of physical permafrost dynamics in the
314 JULES land-surface model. *Geoscientific Model Development* **8**, 1493-1508 (2015).
- 315 25 Burke, E. J., Chadburn, S. E. & Ekici, A. A vertical representation of soil carbon in the
316 JULES land surface scheme (vn4. 3_permafrost) with a focus on permafrost regions.
317 *Geoscientific Model Development* **10**, 959 (2017).
- 318 26 Morice, C. P., Kennedy, J. J., Rayner, N. A. & Jones, P. D. Quantifying uncertainties in
319 global and regional temperature change using an ensemble of observational estimates: The
320 HadCRUT4 data set. *Journal of Geophysical Research: Atmospheres* **117**, D08101,
321 doi:10.1029/2011JD017187 (2012).
- 322 27 Meinshausen, M. *et al.* The RCP greenhouse gas concentrations and their extensions from
323 1765 to 2300. *Climatic Change* **109**, 213, doi:10.1007/s10584-011-0156-z (2011).

- 324 28 van Vuuren, D. P. *et al.* Energy, land-use and greenhouse gas emissions trajectories under
325 a green growth paradigm. *Global Environmental Change* **42**, 237-250 (2017).
- 326 29 Brown, J., Ferrians Jr, O., Heginbottom, J. & Melnikov, E. (National Snow and Ice Data
327 Center, 1998).
- 328 30 Chadburn, S. E. *et al.* An observation-based constraint on permafrost loss as a function of
329 global warming. **7**, 340, doi:10.1038/nclimate3262 (2017).
- 330 31 Zhang, B. *et al.* Methane emissions from global wetlands: An assessment of the
331 uncertainty associated with various wetland extent data sets. *Atmospheric Environment*
332 **165**, 310-321, doi:<https://doi.org/10.1016/j.atmosenv.2017.07.001> (2017).
- 333 32 Poulter, B. *et al.* Global wetland contribution to 2000–2012 atmospheric methane growth
334 rate dynamics. *Environmental Research Letters* **12**, 094013 (2017).
- 335 33 Turetsky, M. R. *et al.* A synthesis of methane emissions from 71 northern, temperate, and
336 subtropical wetlands. *Global Change Biology* **20**, 2183-2197, doi:10.1111/gcb.12580
337 (2014).
- 338 34 Saunio, M. *et al.* The global methane budget 2000–2012. *Earth Syst. Sci. Data* **8**, 697-
339 751, doi:10.5194/essd-8-697-2016 (2016).
- 340 35 Jones, C. *et al.* The HadGEM2-ES implementation of CMIP5 centennial simulations.
341 *Geoscientific Model Development* **4**, 543 (2011).
- 342 36 Zona, D. *et al.* Cold season emissions dominate the Arctic tundra methane budget.
343 *Proceedings of the National Academy of Sciences* **113**, 40-45,
344 doi:10.1073/pnas.1516017113 (2016).
- 345 37 McNorton, J. *et al.* Role of regional wetland emissions in atmospheric methane variability.
346 *Geophysical Research Letters* **43**, 11,433-411,444, doi:10.1002/2016GL070649 (2016).
- 347 38 Clark, D. *et al.* The Joint UK Land Environment Simulator (JULES), model description -
348 Part 2: Carbon fluxes and vegetation dynamics. *Geoscientific Model Development* **4**, 701-
349 722, doi:10.5194/gmd-4-701-2011 (2011).
- 350 39 Gedney, N. & Cox, P. M. The sensitivity of global climate model simulations to the
351 representation of soil moisture heterogeneity. *Journal of Hydrometeorology* **4**, 1265-1275
352 (2003).
- 353 40 Marthews, T., Dadson, S., Lehner, B., Abele, S. & Gedney, N. High-resolution global
354 topographic index values for use in large-scale hydrological modelling. *Hydrology and*
355 *Earth System Sciences* **19**, 91-104 (2015).
- 356 41 Klein Goldewijk, K., Beusen, A., Van Dreht, G. & De Vos, M. The HYDE 3.1 spatially
357 explicit database of human-induced global land-use change over the past 12,000 years.
358 *Global Ecology and Biogeography* **20**, 73-86 (2011).
- 359 42 Sitch, S., Cox, P. M., Collins, W. J. & Huntingford, C. Indirect radiative forcing of climate
360 change through ozone effects on the land-carbon sink. *Nature* **448**, 791-794 (2007).
- 361 43 Stohl, A. *et al.* Evaluating the climate and air quality impacts of short-lived pollutants.
362 *Atmos. Chem. Phys.* **15**, 10529-10566, doi:10.5194/acp-15-10529-2015 (2015).
- 363 44 Etminan, M., Myhre, G., Highwood, E. J. & Shine, K. P. Radiative forcing of carbon
364 dioxide, methane, and nitrous oxide: A significant revision of the methane radiative
365 forcing. *Geophysical Research Letters* **43**, 12,614-612,623, doi:10.1002/2016GL071930
366 (2016).
- 367 45 IPCC. *Climate change 2001: the scientific basis*. (The Press Syndicate of the University
368 of Cambridge, 2001).

369 **Corresponding Author**

370 All correspondence and requests for materials should be made to Edward Comyn-Platt
371 (edwcom@ceh.ac.uk).

372 **Acknowledgements**

373 The work was undertaken as part of the UK Natural Environment Research Council's
374 programme "Understanding the Pathways to and Impacts of a 1.5°C Rise in Global
375 Temperature" through grants NE/P015050/1 CLIFFTOP (E.C-P, G.H., S.C.), NE/P014909/1,
376 MOC1.5 (W.C., C.W., C.H., P.C., S.S.) and NE/P014941/1 CLUES (P.C., T.P.). We also
377 acknowledge the support for: (a) E.B. and N.G., the Joint UK BEIS/Defra Met Office Hadley
378 Centre Climate Programme (GA01101); (b) E.B., CRESCENDO (EU project 641816); (c)
379 A.H., EPSRC Fellowship "Negative Emissions and the Food-Energy-Water Nexus"
380 (EP/N030141/1); and (d) C.H., CEH National Capability Funding. We also acknowledge the
381 wetland extent data products provided by Dr. B. Zhang, of Auburn University, USA and Dr.
382 B. Poulter of the NASA Goddard Space Flight Center, USA.

383 **Author Contributions**

384 G.H., E.B., S.C. and E.C-P conceived and developed the project. E.C-P and C.H. led the
385 development of the inverse IMOGEN model system. E.B. and S.C. contributed code and
386 expertise on permafrost and soil carbon modelling. N.G., S.C. and E.C.P. contributed code and
387 expertise on the JULES wetlands methane scheme. A.H. and T.P. contributed land use change,
388 W.C. and C.W. ozone ancillary data and S.S. contributed expertise on the ozone damage
389 effects, respectively. E.C-P., C.H., G.H., E.B., S.C., W.C., C.W., P.C., A.H. and T.P.
390 contributed to the design of the IMOGEN model runs. All authors contributed to the
391 interpretation of the results and to the writing of the paper.

392 **Competing financial interests**

393 The authors declare no competing financial interests.

394 **Methods**

395 **(1) The JULES model^{20,21}.**

396 **(a) Model version and configuration**

397 JULES is a process-based land surface model that simulates energy, water and carbon fluxes
398 at the land-atmosphere boundary. JULES can be run as a standalone model using given
399 meteorological driving variables or as the land surface component of climate modelling
400 systems of varying degrees of complexity, e.g. Earth System Models³⁵ or IMOGEN¹⁸. We use
401 the JULES version 4.8 release with the addition of a 14 layered soil column over 3m for both
402 hydro-thermal²⁴ and carbon dynamics²⁵. Burke et al.,²⁵ demonstrated that modelling the soil
403 carbon fluxes as a multi-layered scheme improves estimates of soil carbon stocks and net
404 ecosystem exchange. In addition to the vertically discretised respiration and litter input terms,
405 the soil carbon balance also includes a diffusivity term which represents
406 cryoturbation/bioturbation processes. The freeze-thaw processes of cryoturbation is
407 particularly important in cold permafrost type soils¹⁰.

408 The multi-layered methanogenesis scheme improves the representation of high latitude CH₄
409 emissions where previous studies underestimated production at cold permafrost sites during
410 “shoulder seasons”³⁶. The multi-layered scheme allows an insulated sub-surface layer of active
411 methanogenesis to continue after the surface has frozen. These model developments not only
412 improve the seasonality of the emissions, but more importantly for this study capture the release
413 of carbon as CH₄ from deep soil layers, including thawed permafrost. The formulation of the
414 multi-layered scheme gives the local land-atmosphere CH₄ flux, E_{CH_4} (kg C m⁻² s⁻¹), as:

$$E_{CH_4} = k \cdot f_{wetl} \cdot \sum_{C_s \text{ pools}}^i \kappa_i \cdot \sum_{z=0m}^{z=3m} e^{-\gamma z} C_{S_{i,z}} \cdot Q_{10}(T_{soil_z})^{0.1(T_{soil_z}-T_0)}$$

Equation 1

415 Where z is the depth in soil column (in m), i is the soil carbon pool, f_{wetl} (-) is the fraction of
416 wetland area in the gridcell, κ_i (s^{-1}) is the specific respiration rate of each pool (Table 8 of [21]),
417 C_s ($kg\ m^{-2}$) is soil carbon, T_{soil} (K) is the soil temperature. γ ($= 0.4\ m^{-1}$) is a constant that
418 describes the reduced contribution of CH_4 emission at deeper soil layers due to inhibited
419 transport and increased oxidation through overlaying soil layers. This is a simplification,
420 however previous work which explicitly represented these processes showed little to no
421 improvement when compared with in-situ observations³⁷. The four soil carbon pools (i) in
422 JULES are decomposable plant material, resistant plant material, microbial biomass, and
423 humus. As JULES is a processed based model, the carbon emitted as CH_4 is therefore removed
424 from the soil carbon stock. Furthermore, as described in [38], soil respiration is non-zero in
425 fully saturated soils, hence in anaerobic conditions JULES produces CO_2 in addition to CH_4 .

426 f_{wetl} is calculated using the JULES implementation of TOPMODEL³⁹ as the integral of a
427 normalised gamma distribution of a prescribed topographic index dataset⁴⁰, $G(\tau)$, between a
428 critical, τ_{crit} ($\ln(m)$), and maximum, τ_{max} ($\ln(m)$), topographic index, i.e.:

$$f_{wetl} = \int_{\tau_{crit}}^{\tau_{max}} G(\tau) d\tau, \quad \text{Equation 2}$$

429 τ_{crit} is dependent on the local water table as:

$$\tau_{crit} = \ln\left(\frac{\Psi(0)}{\Psi(\bar{z}_w)}\right) + \bar{\tau}, \quad \text{Equation 3}$$

430 where $\Psi(0)$ and $\Psi(\bar{z}_w)$ (m^2s^{-1}) are the transmissivities of entire soil column and the soil column
431 below the mean water table depth, \bar{z}_w (m). The τ_{max} limit excludes regions where the water
432 table is sufficiently high enough for stream flow and hence assumed to be a negligible emitter
433 of CH_4 . It is calculated as:

$$\tau_{max} = \tau_{crit} + \tau_{range}, \quad \text{Equation 4}$$

434 where τ_{range} ($= 2.0$) is a global tuning parameter.

435 \bar{z}_w is incrementally updated based on the balance of water flux processes on each JULES
 436 timestep. When \bar{z}_w is in the deep store (a singular 15 m below the 14 modelled layers) it is
 437 updated as the balance between the infiltration water, I_{Deep} , and the baseflow, B_{Deep} , as:

$$\rho\theta_{sat} \frac{d(\bar{z}_w)}{dt} = I_{Deep} - B_{Deep}, \quad \text{Equation 5}$$

438 where ρ is the density of water and θ_{sat} is the saturated volumetric water content. If the deep
 439 layer is fully saturated \bar{z}_w is calculated diagnostically to be in the deepest unsaturated model
 440 soil layer. The water content of each layer, j , is updated on each time step as the balance of the
 441 vertical flux processes (infiltration, I_j , and Evapotranspiration, E_j), and, for layers below \bar{z}_w , a
 442 horizontal baseflow flux, B_j , i.e.:

$$\Delta z_j \rho \frac{d(\theta_j)}{dt} = I_j - E_j - B_j, \quad \text{Equation 6}$$

443 where Δz_j is the thickness and θ_j is the volumetric water content of j^{th} soil layer. For full details
 444 of the process based JULES hydrology please refer to [20] and [39].

445 In addition, the JULES configuration includes prescribed land-use and land-use change
 446 (LULUC), where land used for agriculture can only grow C3 and C4 grasses to represent crops
 447 and pasture. The land-use mask consists of an annual fraction of agricultural land in each grid
 448 cell. Historical LULUC is based on the HYDE 3.1 dataset⁴¹, and future LULUC is based on
 449 the SSP2_RCP-2.6_IMAGE²⁸. When natural vegetation is converted to managed agricultural
 450 land, the removed vegetation carbon is placed into woody product pools that decay at various
 451 rates back into the atmosphere³⁵. The carbon flux from LULUC is therefore not lost from the
 452 system.

453 We use a JULES configuration including ozone deposition damage to plant stomata, which
 454 then affects land-atmosphere CO₂ exchange⁴². JULES requires surface atmospheric ozone
 455 concentrations, O₃ (ppb), for the duration of the simulation period (1850-2100). Here, we use

456 two sets of monthly O₃ concentration fields calculated using the HADGEM3-A GA4.0 model
457 for low (1285 ppbv) and high (2062 ppbv) global mean atmospheric CH₄ concentrations⁴³. We
458 regrid these fields (1.875°x1.25° horizontal grid) to the spatial grid of IMOGEN-JULES
459 (3.75°x2.5° horizontal grid). We then linearly interpolate between the respective months in the
460 regridded O₃ fields using the global annual atmospheric CH₄ concentration. The CH₄
461 concentration is taken from the prescribed SSP2_RCP-2.6_IMAGE plus the natural CH₄
462 modulation when the interactive scheme is in use.

463 **(b) Wetland CH₄ emission scheme calibration**

464 We calibrate the temperature sensitivity of the multi-layered methanogenesis scheme (k and
465 $Q_{10}(T_{soil}) = Q_{10}^{[T_0/T_{soil}]}$ in Equation 1) for each CMIP5 model in the IMOGEN ensemble to
466 ensure the wetland CH₄ production rates match present day observations^{33,34}. [33] fit observed
467 surface CH₄ fluxes, E_{CH_4} , against temperature to Equation 7 using data from 71 sites:

$$E_{CH_4, Turetsky} = A_{Turetsky} \times Q_{10, Turetsky}^{0.1T_{soil-10cm}}, \quad \text{Equation 7}$$

468 where $T_{soil-10cm}$ is the temperature of the top 10 cm of soil.

469 To capture temperature sensitivity uncertainty we calibrate Q_{10} in Equation 1 against Equation
470 7 for 2 of the wetland types identified in [33] (“Poor Fen” and “Rich Fen”) using the daily output
471 from the JULES-simulations at the year 2000 for each GCM. We select Q_{10} values which
472 maximise the Pearson’s correlation coefficient. k is then calculated such that the global total
473 for the year 2000 is 180 TgCH₄ to match our assumptions of the atmospheric growth rate of
474 CH₄ in the IMOGEN CH₄ feedback calculations (see IMOGEN description below). We
475 selected the “Poor Fen” and “Rich Fen” parameterisations for our ensemble as these gave the
476 best representation of the global distribution of CH₄ emissions when compared with the output
477 from [34] (Figure SI.9). A “Bog” parameterisation was ruled out as this tended towards
478 unrealistically high tropical emissions, a “Swamp” parameterisation was ruled out due to the

479 high levels of uncertainty reported in [33]. The optimised parameter values are given in Table
480 SI.2 of the Supplementary Information. In addition to the two calibrated parameterisations we
481 include a “lowQ₁₀” ($Q_{10}=2.0$, $k=1.625\times 10^{-9}$) parameterisation which gave a larger fraction of
482 global emissions to lower temperature regions (Figure SI.9).

483 **(2) IMOGEN, EBM Inversion and the CMIP5 models selected for its calibration.**

484 **(a) IMOGEN²³** is a climate-carbon cycle model of intermediate complexity that uses “pattern-
485 scaling” of the seven meteorological variables required to drive JULES. Huntingford, et al. ²³
486 assume that changes in local temperature, precipitation, humidity, wind-speed, surface
487 shortwave and longwave radiation and pressure are linear in global warming. Patterns are
488 multiplied by the amount of global warming over land, ΔT_L , to give local monthly predictions
489 of climate change. When using IMOGEN in forward mode, ΔT_L is calculated with an Energy
490 Balance Model (EBM) as a function of the overall changes in radiative forcing, ΔQ (W m^{-2}).
491 ΔQ is the sum of the atmospheric greenhouse gas contributions⁴⁴, updated on a yearly timestep.
492 Our simulations include a CH₄ feedback system that captures the climate impacts on CH₄
493 emissions from natural wetland sources. The approach here follows that of [8] where prescribed
494 CH₄ concentrations, which assume a non-varying natural wetland CH₄ component²⁸, are
495 perturbed using the anomaly in modelled natural wetland CH₄ emission. To ensure consistency
496 with the observed atmospheric CH₄ growth rate we calibrate our model to produce 180 TgCH₄
497 per year for the year 2000, as detailed in the model calibration description above. The
498 increased/reduced atmospheric CH₄ concentration will have corresponding longer/short
499 atmospheric lifetime, λ , than the prescribed concentration pathway. We account for changes in
500 λ following the formulation and parameterisation of [45], i.e. $\lambda=8.4 \text{ yr}^{-1}$ for an atmospheric CH₄
501 concentration of 1745ppb. The changes in radiative forcing were calculated using the
502 formulation in [44]. There is large uncertainty in the natural wetland contribution to global CH₄

503 emissions, for this study we scale to 180 TgCH₄ per year, approximation based on a recent
 504 model intercomparison study³⁴ (Figure SI.6). Additionally, the effect of increased atmospheric
 505 CH₄ concentrations on tropospheric ozone levels is also accounted for, both in terms of
 506 radiative forcing and the impact on surface functioning through stomatal damage (see JULES
 507 description in Methods section 1a).

508 Previous IMOGEN studies^{23,10} used 22 of the Earth System models (ESMs) involved in CMIP3
 509 (phase 3 of the Coupled Model Intercomparison Project). Here, we update and extend
 510 IMOGEN to use Earth System models (ESMs) involved in CMIP5. We downloaded CMIP5
 511 data from the mirror database held on the UK JASMIN computer during Autumn 2015. Table
 512 SI.1 lists every model for which historical monthly *surface temperature* fields were available.
 513 The key criteria for inclusion of the output from a given CMIP5 GCM simulation is as follows
 514 (see Supplementary Information and Table SI.1):

- 515 1. Availability for the internal Energy Balance Model of surface temperature, top of the
 516 atmosphere (TOA) incoming shortwave radiation, outgoing TOA shortwave and longwave
 517 radiation;
- 518 2. Availability of meteorological parameters to drive JULES: surface temperature,
 519 precipitation, surface relative humidity, surface downward shortwave radiation, surface
 520 downward longwave radiation, surface wind speeds and surface pressure
- 521 3. Availability of two RCP scenarios for calibration and testing

522 **(b) Energy Balance Model (EBM) Inversion.** The EBM was inverted such that a change in
 523 radiative forcing, ΔQ , is calculated as a function of a change in the global temperature, ΔT_g
 524 (K), re-ordering of Equation (10) from Huntingford and Cox²² gives:

$$\Delta Q(t) = f \left[\Delta T_o \left[\frac{(1-f)\lambda_l \nu}{f} + \lambda_o \right] - \kappa \frac{\partial \Delta T_{o,s}}{\partial z} \Big|_{z=0} \right], \quad \text{Equation 8}$$

525 Where $\Delta Q(t)$ is the change in radiative forcing (W m^{-2}) at time t , f is the fraction of Earth that
 526 is ocean, λ_l and λ_o are the climate sensitivities over land and ocean, respectively ($\text{W m}^{-2} \text{K}^{-1}$), ν
 527 is the land-sea contrast and κ is the ocean diffusivity ($\text{W m}^{-1} \text{K}^{-1}$). The values of the parameters
 528 f , λ_l , λ_o , ν and κ are unique to each GCM in the ensemble and are listed in the Supplementary
 529 Information, Table SI.2.

530 The change in the depth-dependent ocean temperature (ΔT_o) (K) must satisfy the diffusivity
 531 equation:

$$c_p \frac{\partial \Delta T_{o,s}}{\partial t} = \kappa \frac{\partial^2 \Delta T_{o,s}}{\partial z^2}, \quad \text{Equation 9}$$

532 where c_p is ($\text{J K}^{-1} \text{m}^{-3}$) is the specific heat capacity of salt water and z (m) is ocean depth
 533 (positive downwards). The change in the global mean surface ocean temperature ($z=0$) is then
 534 calculated from the global temperature, ΔT_G as ²²:

$$\Delta T_o = \frac{\Delta T_G}{[f + \nu - f\nu]}. \quad \text{Equation 10}$$

535 The global mean land temperature, ΔT_L , required for the “pattern scaling” was calculated as:

$$\Delta T_L = \nu \Delta T_o \quad \text{Equation 11}$$

536 (c) Etminan CO₂ Radiative Forcing Inversion.

537 Etminan et al.⁴⁴ present a formulation to calculate the change in radiative forcing, ΔQ_{CO_2} , from
 538 a given change in the global mean atmospheric CO₂ concentration. There is no exact solution
 539 for the inverse of this, i.e. to calculate the change in CO₂ for a given ΔQ_{CO_2} . We find the solution
 540 iteratively using Equation 3:

$$CO_{2i+1} = CO_{2REF} \times e^{\left[\frac{\Delta Q_{CO_2}}{a_1(CO_{2i} - CO_{2REF})^2 + b_1(CO_{2i} - CO_{2REF}) + c_1\bar{N} + 5.36} \right]} \quad \text{Equation 12}$$

541 We assume convergence has occurred if the CO₂ concentration changes by less than 0.001
542 ppm. The initial CO₂ concentration for the iteration is taken to be the CO₂ concentration for
543 the previous year. We typically find that no more than 5 iterations are required for a change of
544 10 ppm from the starting concentration.

545 **(d) Q non-CO₂ calculation.** Changes in radiative forcing, ΔQ (Wm⁻²), calculated by the
546 inverted IMOGEN EBM must be ascribed to changes in the atmospheric composition of GHGs.
547 For this simplified description we consider two forcing contributions. The CO₂ forcing, ΔQ_{CO_2}
548 (Wm⁻²), and the forcing of all other agents, ΔQ_{nonCO_2} (Wm⁻²). In the simplest case (not
549 considering interactive CH₄), a prescribed ΔQ_{nonCO_2} , is removed from ΔQ to give ΔQ_{CO_2} as:

$$\Delta Q_{CO_2} = \Delta Q - \Delta Q_{non\ CO_2}. \quad \text{Equation 13}$$

550 The non-CO₂ composition is taken from the SSP2_RCP-2.6_IMAGE pathway²⁸. The
551 SSP2_RCP-2.6_IMAGE pathway was chosen as it assumes very high GHG mitigation and the
552 global warming pathway is reasonably close to the 1.5°C or 2.0°C targets of interest (i.e. 1.8
553 °C by 2100). This prescribed non-CO₂ radiative forcing is subtracted from ΔQ to give the CO₂
554 radiative forcing ($\Delta Q_{CO_2} = \Delta Q - \Delta Q_{non\ CO_2}$). The CO₂ concentration is then derived using an
555 iterated inversion of the CO₂ radiative forcing equation in Etminan et al.⁴⁴ (Methods). For a
556 given $\Delta Q_{non\ CO_2}$, we then estimate the CO₂ concentration iteratively, as described above, using
557 Equation 3.

558 Each of the 34 GCMs that IMOGEN emulates has a different set of EBM parameters - λ_1 , λ_o , ν ,
559 κ and f . Hence each GCM has a different ΔQ estimate for a given $\Delta T_G(t)$ pathway. When
560 IMOGEN is driven with a historical record of ΔT_G the range of ΔQ for the present day (2015)
561 is 1.13 W m⁻² (Supplementary Information Figure SI.5a). For this work, we require the
562 historical period, 1850-2015, to match observations of both ΔT_G and atmospheric composition
563 for all GCMs. We, therefore, attribute the spread in ΔQ to uncertainty in $\Delta Q_{non\ CO_2}$, particularly

564 the atmospheric aerosol contribution which has an uncertainty range of -0.5 to -4 Wm⁻². Given
 565 this, and to ensure continuous functions of ΔQ_{CO_2} and $\Delta Q_{non\ CO_2}$, we calculated the contributions
 566 as:

$$\Delta Q_{CO_2}(t) = \begin{cases} \Delta Q_{CO_2}(t)_{SSP}, & t \leq 2015 \\ \Delta Q(t) - \Delta Q_{non\ CO_2}(t), & t > 2015 \end{cases}$$

$$\Delta Q_{non\ CO_2}(t) = \begin{cases} \Delta Q(t) - \Delta Q_{CO_2}(t)_{SSP}, & t \leq 2015 \\ \Delta Q_{non\ CO_2}(t)_{SSP} + c(GCM), & t > 2015 \end{cases}$$

Equation 14

567 where the subscript SSP indicates the value is sourced from SSP2_RCP-2.6_IMAGE. c (Wm⁻²)
 568 ²) is a GCM specific offset which ensured continuous ΔQ_{CO_2} or $\Delta Q_{non\ CO_2}$ and was calculated
 569 at the transitional year (2015) as:

$$c(GCM) = \Delta Q_{non\ CO_2}(2015) - \Delta Q_{non\ CO_2}(2015)_{SSP}$$

Equation 15

570 Figure SI.5 in the supplementary information shows the allocation of the ΔQ and the resultant
 571 atmospheric CO₂ concentration pathways for the 2°C stabilisation temperature. We include the
 572 GCM specific 2015 aerosol-offsets in Table SI.2 in the Supplementary Information.

573 **(3) Temperature Profile Formulation.** [19] provides a framework to create temperature
 574 trajectories based on two parameters which model the efforts of humanity to limit emissions
 575 and, if necessary, capture atmospheric carbon, i.e.:

$$\Delta T(t) = \Delta T_0 + \gamma t + (1 - e^{-\mu(t)t})[\gamma t - (\Delta T_{Lim} - \Delta T_0)]$$

Equation 16

576 where, $\Delta T(t)$ is the change in temperature from pre-industrial levels at year t , ΔT_0 is the
 577 temperature change at a given initial point (in this case $\Delta T_0 = 0.89^\circ\text{C}$ for 2015), ΔT_{Lim} is the
 578 final prescribed warming limit and:

$$\mu(t) = \mu_0 + \mu_1 t,$$

Equation 17

$$\gamma = \beta - \mu_0(\Delta T_{\text{Lim}} - \Delta T_0).$$

579 Where β (= 0.00128) is the current rate of warming and the μ_0 and μ_1 are tuning parameters
 580 which describe anthropogenic attempts to stabilise global temperatures¹⁹. The selected
 581 parameterisation of the three trajectories are based on comparisons with CMIP5 simulations
 582 for the RCP2.6 scenario (grey lines in Figure SI.2). The parameter values used for the three
 583 profiles selected are shown below.

Profile	ΔT_{lim}	μ_0	μ_1
1.5°C	1.5	0.1	0.0
1.5°C (overshoot)	1.5	-0.01	0.00085
2°C	2.0	0.08	0.0

584

585 (4) Code and Data Availability

586 The data that support the findings of this study are available from the corresponding author
 587 upon request.

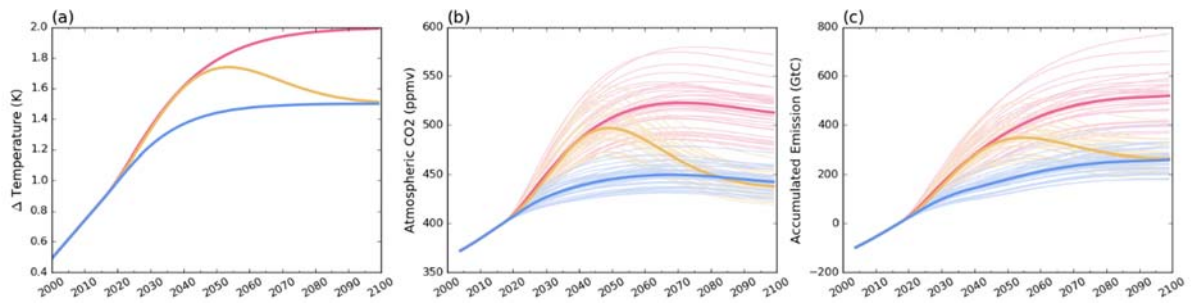
588 JULES is an open-source model and the code branch used in this work is available from the
 589 met-office science repository using the following URL (registration required):

590 https://code.metoffice.gov.uk/trac/jules/browser/main/branches/dev/edwardcomynplatt/vn4.8_1P5_DEGREES?rev=11764

592 The parameterisations used herein are also permanently stored on the met-office science
 593 repository. Given the complexities in accessing the specific revision and machine configuration
 594 required, these will be made available upon request to the corresponding author.

595

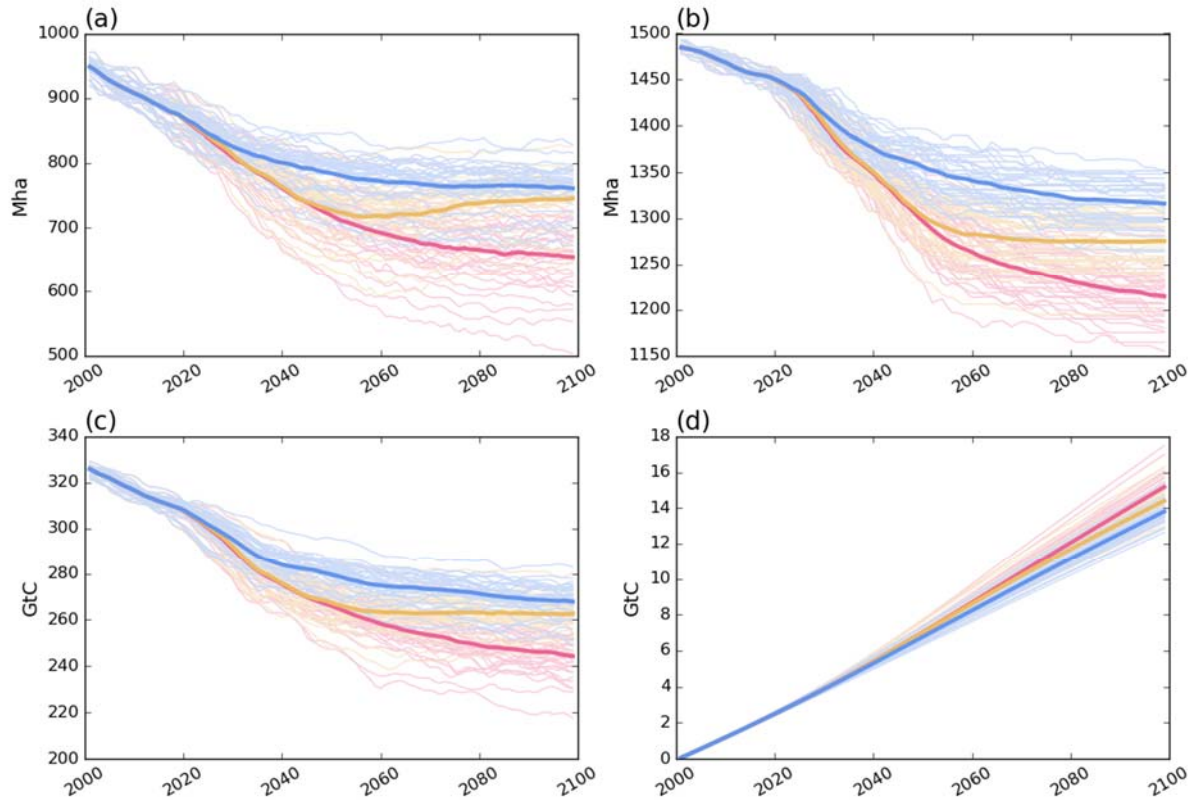
596 **Figure Captions**



597

598 *Figure 1 Time-series for the control model ensemble. Blue is the 1.5°C asymptote pathway, yellow is the 1.5°C overshoot*
599 *pathway and red is the 2°C asymptote pathway. Faint lines are the individual GCMs, bold lines represent the ensemble median,*
600 *and the colours are consistent across the panels. (a) Temperature pathways; (b) simulated atmospheric CO₂ concentrations;*
601 *(c) derived allowable anthropogenic emissions.*

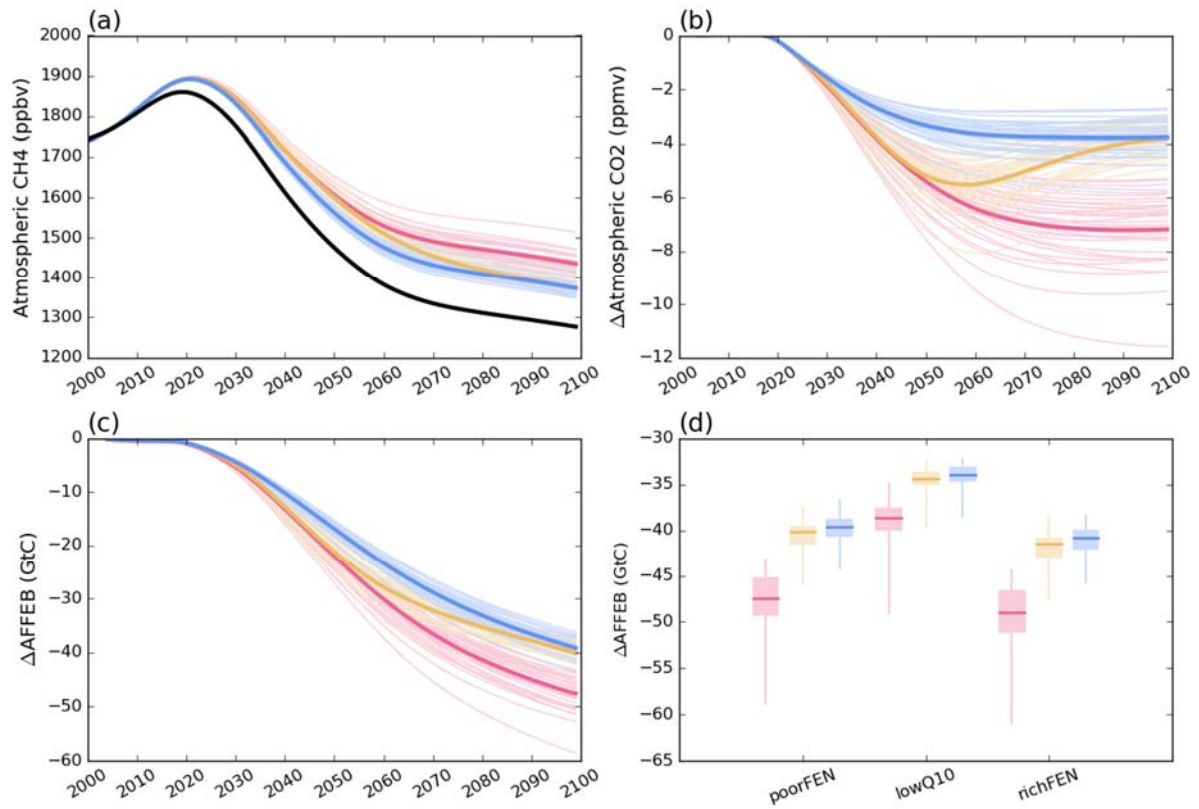
602



603

604 *Figure 2 The response of the permafrost soil column to warming through the 21st century. (a) Areal extent of permafrost within*
605 *the top 1m of soil column; (b) areal extent of permafrost within the top 3m of soil column; (c) the amount of pre-industrial*
606 *permafrost carbon still perennially frozen; (d) the amount of pre-industrial carbon lost to the atmosphere. Blue is the 1.5°C*
607 *asymptote pathway, yellow is the 1.5°C overshoot pathway and red is the 2°C asymptote pathway*

608



609

610

611

612

613

614

615

Figure 3 Summary results for the natural methane feedback experiment. (a) Time-series of atmospheric CH₄ when the interactive natural CH₄ is included (“poor fen” parameterisation) for the three temperature pathways. The black line is the control simulation atmospheric CH₄. (b) The reduction in atmospheric CO₂ (from control simulation) to follow the prescribed temperature pathway. (c) The reduction in anthropogenic fossil fuel emissions due to reduced atmosphere, land and ocean sinks. (d) The reduction in AFFEB for the temperature sensitivity uncertainty ensemble. Blue is the 1.5°C asymptote pathway, yellow is the 1.5°C overshoot pathway and red is the 2°C asymptote pathway.

616

617 **Tables**

618 *Table 1 Emission budgets from the factorial experiment and the changes due to the introduction of the feedback processes.*
 619 *White cells represent the absolute emission budget for the 2015-2100 period, blue cells represent the change due to inclusion*
 620 *of carbon released from the permafrost store, yellow cells represent the change due to inclusion of an interactive CH₄ scheme*
 621 *and green cells represent the change due to inclusion of both permafrost and interactive CH₄ feedbacks. Bold values give the*
 622 *climate ensemble median for the “poor fen” CH₄ parameterisation. Bracketed values represent the spread of the climate*
 623 *ensemble interquartile ranges for the 3 temperature sensitivity experiments (i.e. the full spread of the boxes in Figure 3d).*

Total anthropogenic fossil fuel CO₂ emissions (GtC)				
		Standard	Methane Feedback	Difference
1.5°C	Standard	265 (226-283)	226 (187-249)	39.6 (33.1-42.1)
	Permafrost Feedback	254 (214-276)	214 (175-235)	40.1 (34.7-42.4)
	Difference	11.9 (11.6-12.2)	12.5 (11.9-14.0)	52.1 (46.6-54.2) 19.4 % (16.7-22.9 %)
1.5°C overshoot	Standard	271 (227-288)	232 (185-254)	40.2 (33.6-42.8)
	Permafrost Feedback	258 (214-276)	218 (172-240)	40.6 (36.3-43.1)
	Difference	12.5 (12.1-13.0)	13.0 (12.4-14.3)	53.5 (47.4-55.7) 19.5 % (16.6-23.2 %)
2°C	Standard	527 (464-568)	504 (417-528)	47.4 (37.3-51.0)
	Permafrost Feedback	514 (451-554)	467 (404-514)	47.8 (38.6-51.3)
	Difference	13.3 (12.8-13.8)	13.6 (13.0-15.0)	61.1 (51.4 -64.6) 11.4 % (9.5-13.0 %)

624

625

626